


Article

Morphological Characteristics and Printing Mechanisms of Grid Lines by Laser-Induced Forward Transfer

Yanmei Zhang^{1,2,3}, Chongxin Tian^{1,3,4}, Yucui Yu^{1,3}, Xiuli He^{1,3,4}, Yanhua Bian^{1,3}, Shaoxia Li^{1,3,4,*} 
and Gang Yu^{1,2,3,4,*}

¹ Institute of Mechanics, Chinese Academy of Sciences, Beijing 100190, China

² Center of Materials Science and Optoelectronics Engineering, University of Chinese Academy of Sciences, Beijing 100049, China

³ School of Engineering Science, University of Chinese Academy of Sciences, Beijing 100049, China

⁴ Guangdong Aerospace Research Academy, Guangzhou 511458, China

* Correspondence: lisx@imech.ac.cn (S.L.); gyu@imech.ac.cn (G.Y.)

Abstract: Laser-induced forward transfer (LIFT) is an innovative metallization technique used in the processing of grid lines of solar cells for the photovoltaics industry. A study on the morphology and transfer mechanisms of formed lines with high-viscosity silver paste and small gap was performed in this paper. There were three different transfer states under different laser fluences: non-transferred lines or transferred but no continuous lines, continuous transferred lines, and explosive transferred lines. There was a critical transfer threshold for the continuous line transfer under different processing speeds. Higher processing speed required a larger critical transfer threshold. The line width increased as the laser fluence increased. For all continuous formed lines, the cross-sectional morphologies with single and double peaks were shown at critical and above transfer threshold, respectively. Two symmetrical protrusions with steep edges were observed for the formed line with double peaks. By comparing the silver paste remaining on the donor and transferred to the acceptor under different laser fluences, it can be found the transferred silver paste exhibited a retracting characteristic under the critical and above transfer threshold. While a stretching characteristic was obvious when the laser fluence was much higher than the transfer threshold. Morphological characteristics with single or double peaks were determined by the distance between the rupture position of the bridge and the bottom of the bubble, under the action of the axial combined forces. This work can provide insights for improving fine-line metallization and understanding transfer mechanisms in the photovoltaic application and flexible electronics devices.

Keywords: laser-induced forward transfer (LIFT); grid lines; morphology; transfer mechanism; metallization



Citation: Zhang, Y.; Tian, C.; Yu, Y.; He, X.; Bian, Y.; Li, S.; Yu, G.

Morphological Characteristics and Printing Mechanisms of Grid Lines by Laser-Induced Forward Transfer. *Metals* **2022**, *12*, 2090. <https://doi.org/10.3390/met12122090>

Academic Editor: Pavel Krakhmalev

Received: 14 October 2022

Accepted: 29 November 2022

Published: 6 December 2022

Publisher's Note: MDPI stays neutral with regard to jurisdictional claims in published maps and institutional affiliations.



Copyright: © 2022 by the authors. Licensee MDPI, Basel, Switzerland. This article is an open access article distributed under the terms and conditions of the Creative Commons Attribution (CC BY) license (<https://creativecommons.org/licenses/by/4.0/>).

1. Introduction

Solar cells are used to convert the renewable solar energy into electric energy via the photovoltaic technology. Conductive grid lines are indispensable for the front-side and rear-side metallization of solar cells [1]. Many technological issues have been faced, especially while fabricating grid lines with narrow width and high aspect-ratio to reduce the shading loss and increase short circuit current. Screen printing is a traditional and mature manufacturing technology in this field [2,3]. Because there is direct contact with the silicon wafer in the printing process, the breakage of silicon wafer is inevitable, especially with the development of thin silicon wafers. Furthermore, screen clogging and silver paste waste may occur when the high-viscosity silver paste is transferred [4].

Currently, laser-induced forward transfer (LIFT) on grid lines of solar cells is an innovative metallization technique. It has the advantages of non-mask and non-contact printing [5]. The possibility of silicon wafer breakage and paste clogging can be eliminated. Moreover, there are few constraints concerning viscosity and particle size of the transferred materials [4,6]. In addition, the processing efficiency will be increased due to the high flexibility of laser and

the consumption of silver paste is significantly reduced. All these attractive features have made LIFT feasible for industrial implementation of solar cell metallization [7,8].

Inks and paste with low viscosity and solid content are usually used as the transferred materials for LIFT. A commercial silver paste with nominal viscosity of 12.7 Pa·s and solid content of 74.1% was used to print single voxels [4]. The linear dependence of voxel volume on different laser energies and large gaps from 200 μm to 600 μm was analyzed. When the laser pulse was absorbed, a bubble was induced which could expand and retract without jet propulsion. Deposits appeared through bubble contact with the acceptor. A conductive ink with a viscosity of 10–13 mPa·s was used to investigate different behaviors of multi-jet formation and transferred droplets [9]. It was demonstrated that an expanded bubble in the liquid was generated which propelled a jet towards the acceptor under a large gap. A 30 μm thick liquid ink was prepared on the donor, with a relatively large distance (1 mm) from the acceptor [10]. Various inter-beam separations were carried out to analyze both the printing droplets and the corresponding liquid transfer dynamics. Usually in these studies, a big gap, low-viscosity and thick donor film were set for the transfer process to visualize the jet dynamics and characterize the formed lines. An investigation focused on the LIFT process with a small-gap and high-viscosity silver paste is still lacking.

Several studies have been conducted to explore the parametric window for optimum printing of the formed lines with narrow width and high aspect-ratio. Shan et al. [1] obtained a continuous line with the width of 44 μm and aspect-ratio of 0.54 by using the optimal parameters in the single-step printing process. The width and aspect-ratio of the formed lines were compared using silver paste with different viscosities (250 Pa·s and 50 Pa·s), and it was revealed that high-resolution continuous lines could only be achieved at the viscosity of 50 Pa·s. Anierte et al. [11] successfully transferred optimized lines with the width of 65 μm and height of 35 μm at the fixed gap of 250 μm . The silver paste was used with a viscosity of 40–70 Pa·s and solid content of 78–80%. The optimal paste thickness was 50 μm in this paper. Shan et al. [12] used the silicon wafer as the acceptor and firstly processed it into a laser-etched double groove structure to restrict the contact area between the silver paste and acceptor. The optimal formed line was obtained at the silver paste viscosity of 25 Pa·s, with an average width of 30.5 μm and aspect-ratio of 0.97 in this paper. It can be found most of these studies often started with the transfer of voxels.

Previous studies demonstrated the feasibility of transferring droplets and lines under large gaps using low-viscosity liquids or paste by LIFT. It is important to understand the transfer dynamics and find the right process parameter range for the continuous line transfer. It is still a great challenge to reduce the width of the continuous formed lines, due to lack of overall understanding about the dependence of forming characteristics on process parameters and silver paste transfer process. During the transfer process, the gap and viscosity are the key constraints and determinants, strongly affecting the morphology and transfer mechanisms of the formed lines. Therefore, it is necessary to regulate them from small to large gap with high precision. In addition, the morphology and transfer mechanisms with a small gap and high-viscosity silver paste, can be readily distinguished from those observed previously under large gaps and low-viscosity liquids, which are urgent to be exploited and studied in depth.

In the present work, a study on transferring high-viscosity silver paste using a small gap was conducted. The formed lines were observed under different laser fluences and processing speeds to determine how the process parameters affect the geometric morphology. Moreover, morphological characteristics of the silver paste remaining on the donor and transferred to the acceptor were compared, aiming at achieving a better understanding of the transfer dynamics. This study will provide insights on improving fine-line metallization in the photovoltaic application.

2. Experimental Setup and Materials

In this paper, all experiments were conducted on a laser precision machining system. The whole device consists of a diode-pumped solid-state laser, optical path system, three-

dimensional platform and computer control system. The pulse width of the laser beam is 10–12 ps and the laser wavelength is 532 nm. The maximum repetition rate of the Gaussian beam is up to 1 MHz. The maximum processing speed is 5 m/s on a predetermined trajectory. The laser beam is focused on the interface between the donor and silver paste. By adjusting the distance between the focusing plane and the donor, the diameter of the laser beam can be varied as the desired. The beam diameter on the donor is 30 μm .

A commercial metallization silver paste was used as the donor material for the laser-induced forward transfer. Table 1 shows the physical and chemical properties of the silver paste. It is a kind of high-temperature and high-viscosity conductive silver paste with the excellent electrical and sintering properties. It is mainly composed of suspending micron-size silver powders and glass powders and organic carrier. Silver powders mainly play a conductive role. Glass powders, as the adhesion binder, are used for coating curing and improving adhesion after sintering. Organic carrier is used as leveling and thixotropic agents to disperse the silver and glass powders.

Table 1. Physical and chemical properties of the silver paste.

Properties	Value
Solid content	90–92%
Average fineness	3–5 μm
Viscosity	160–350 Pa·s

Considering the non-Newtonian fluid properties of the silver paste, it was stirred gently for nearly 10–15 min to ensure the uniformity of viscosity before the usage. Then it was coated onto a laser-transparent substrate to form the specific thickness on the donor. The silver paste was in a state of complete wetting after coating. In this paper, the actual paste thicknesses could be changed from 10 μm to 20 μm , which were measured before and after experiments by laser scanning confocal microscopy (LSCM). Moreover, the film thickness was fixed for all the experiments with a 2 μm fluctuation.

The silicon wafer was chosen as the acceptor just under the silver paste, which was with the average line roughness of 0.3 μm . The distance between the donor and acceptor could be adjusted from 10 μm to 100 μm , with an adjustment accuracy of 5 μm . After the sample preparation, it is necessary to carry out the experiments quickly to ensure the accuracy of the results because the liquid organic carrier is easy to evaporate, which may change the actual viscosity of the silver paste with a high solid content. A schematic diagram of laser-induced forward transfer and the silver paste coated on the donor is shown in Figure 1.

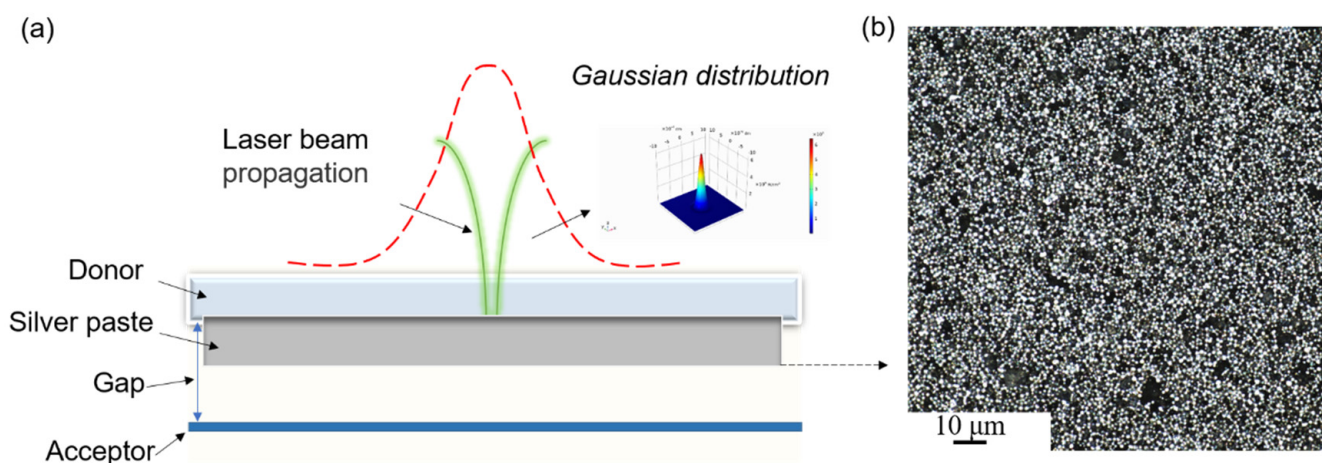


Figure 1. (a) schematic diagram of laser-induced forward transfer, (b) silver paste coated on the donor.

For all experiments, the laser repetition rate was the same, which was set at 1 MHz. The gap between the donor and acceptor was fixed at 25 μm . The processing speeds were set at 1000 mm/s, 2500 mm/s, and 5000 mm/s. Laser fluences were varied from 0.65 J/cm² to 1.56 J/cm², which refer to average fluences. Five lines were transferred for each set of processing parameter in order to ensure the stability and reliability of results. After the experiments, in order to evaporate the solvents and bond the silver powders, silicon wafers were subsequently treated in a box drying oven and sintering furnace to obtain the final transferred grid lines. The drying temperature was at 200 °C and the sintering temperature was at 750 °C, which were provided by the wafer manufacturer. Morphologic characteristics of the formed silver lines were observed and measured by an optical microscope and LSCM. The average of the three positions of the formed line was selected as the final result to reduce the experimental error. Furthermore, the remaining silver paste on the donor was also observed to evaluate the morphology of transferred silver paste under irradiation zones just after the experiments.

3. Results and Discussion

3.1. Width, Height and Aspect-Ratio of Formed Lines

The geometric topography of the formed lines on silicon wafers is important for the conductive performance and conversion efficiency of solar cells. Width, height and aspect-ratio (height over width) are three key parameters to characterize the morphology of the formed lines. For the front-side and rear-side metallization of solar cells, narrow lines will lead to a small area occupied by silver lines on the silicon wafer. Large line height can result in low electrical resistance. It is helpful to save silver paste cost and reduce contact resistance of the solar cell, so that the conversion efficiency of solar energy can be further improved.

Figure 2 shows the two-dimensional morphology of the formed lines under different laser fluences and processing speeds. The laser fluences varied as processing speeds were 5000 mm/s, 2500 mm/s and 1000 mm/s, respectively. For all the formed lines, it could be noticed that there was a matching relationship between the laser fluence and processing speed for the continuous line transfer. There was a relationship among the critical fluence, overlap distance and processing speed for printing. The overlap rate refers to the distance between center of spots compared with their diameter, which was calculated by Equation (1).

$$o = 1 - \frac{v}{2rf} \quad (1)$$

where o is the overlap rate and v is the processing speed. r and f are the beam radius and repetition rate, respectively, which are fixed in this paper. From the Equation (1), it can be concluded that the overlap rate decreased from 96.7% to 83.3% when the processing speed increased from 1000 mm/s to 5000 mm/s. The lower the overlap rate, the more laser fluence was required. This was because the laser fluence of two adjacent laser pulses decreased with the decrease of overlap rate for the transfer of continuous lines. Thus, more laser fluence was needed to transfer silver paste of the same volume for the lower overlap rate.

At the same processing speed, the width of formed line increased as the laser fluence increased. At each processing speed, there was a critical transfer threshold, defined as the threshold fluence at which the silver paste was transferred continuously and the silver line was formed without interruption. The critical laser fluence for each processing speed in Figure 2 was the explored energy density. At the processing speeds of 5000 mm/s, 2500 mm/s and 1000 mm/s, the critical transfer thresholds were 1.32 J/cm², 0.96 J/cm², and 0.65 J/cm², respectively. It can be concluded that the critical transfer threshold depended on the processing speed, with a larger threshold for the higher processing speed. When the laser fluence was less than this critical value, the line was transferred discontinuously. As the laser fluence decreased, there were dots transferred and no silver paste was even transferred to the silicon wafer, as shown in Figure 3a. Conversely, when the laser fluence was over the critical value, more silver paste was transferred under higher energy density. As a result, the formed line became wider. As the laser fluence increased, a large amount

of silver paste was transferred down explosively. There were micro-clusters of the silver paste with small height and random distribution presented on the silicon wafer, as shown in Figure 3b. The results were similar to those described in the literature [4,5,11]. Under lower laser fluences, no transfer and the voxels consisting of non-continuous clusters of silver paste were observed. Under higher laser fluences, the transfer was similar to a splash. Especially a large number of small droplets were away from the center of the laser beam, resulting in a formation of the line with a large width, small height and aspect ratio. Therefore, an appropriate range of the laser fluence is necessary to ensure the continuity of the formed line.

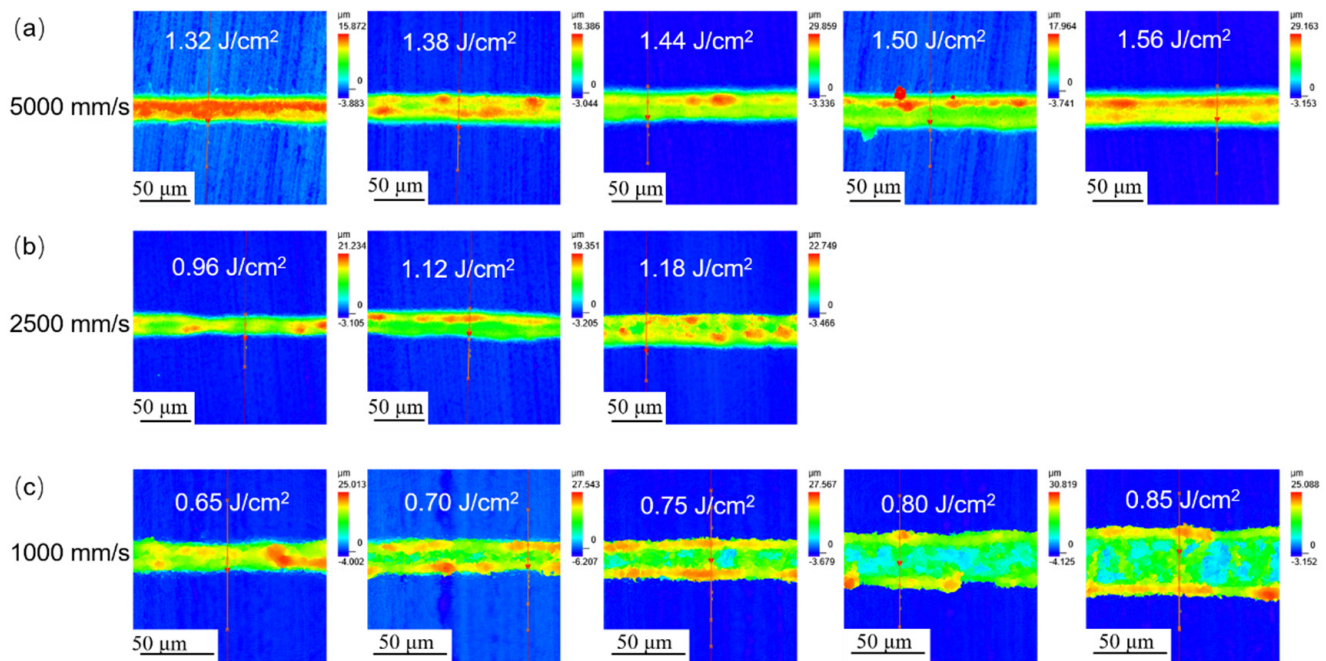


Figure 2. Two-dimensional morphology of the formed lines under different laser fluences and processing speeds obtained by LSCM. (a) 1.32–1.56 J/cm², 5000 mm/s, (b) 0.96–1.18 J/cm², 2500 mm/s, (c) 0.65–0.85 J/cm², 1000 mm/s.

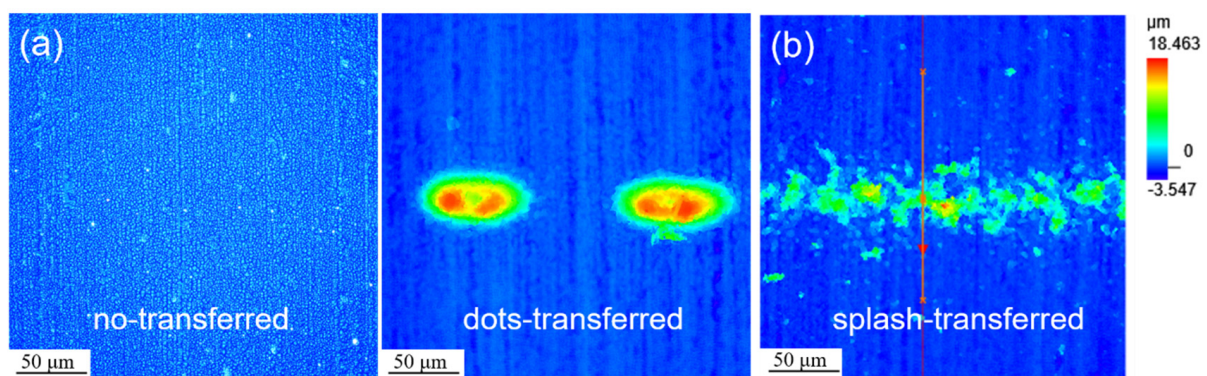


Figure 3. Two-dimensional morphology of the formed lines under lower and higher laser fluences obtained by LSCM. (a) lower fluences: no-transferred or dots transferred, (b) much higher fluences: splash-transferred.

Figure 4 shows the width, height and aspect-ratio of the formed lines under different laser fluences at the processing speeds of 1000 mm/s, 2500 mm/s, and 5000 mm/s. It can be noticed that the narrow line width, large line height and aspect-ratio were shown at the low laser fluences (<0.8 J/cm²), for the processing speed of 1000 mm/s. Even the line

width and line height were almost the same and aspect-ratio reached 1 at the laser fluences of 0.65 J/cm^2 and 0.70 J/cm^2 . For the processing speeds of 2500 mm/s and 5000 mm/s , the minimum widths of the formed lines were larger than $30 \text{ }\mu\text{m}$ and $40 \text{ }\mu\text{m}$, respectively. The line height fluctuated between $10 \text{ }\mu\text{m}$ and $20 \text{ }\mu\text{m}$. All the aspect ratios of the formed line were less than 0.5, but the fluctuation was smaller than that at 1000 mm/s . It can be found that, as the laser fluence increased, the width of the formed line increased significantly compared with the increase of line height. Thus, the aspect ratio showed a remarkable trend of decrease, as shown in Figure 4b.

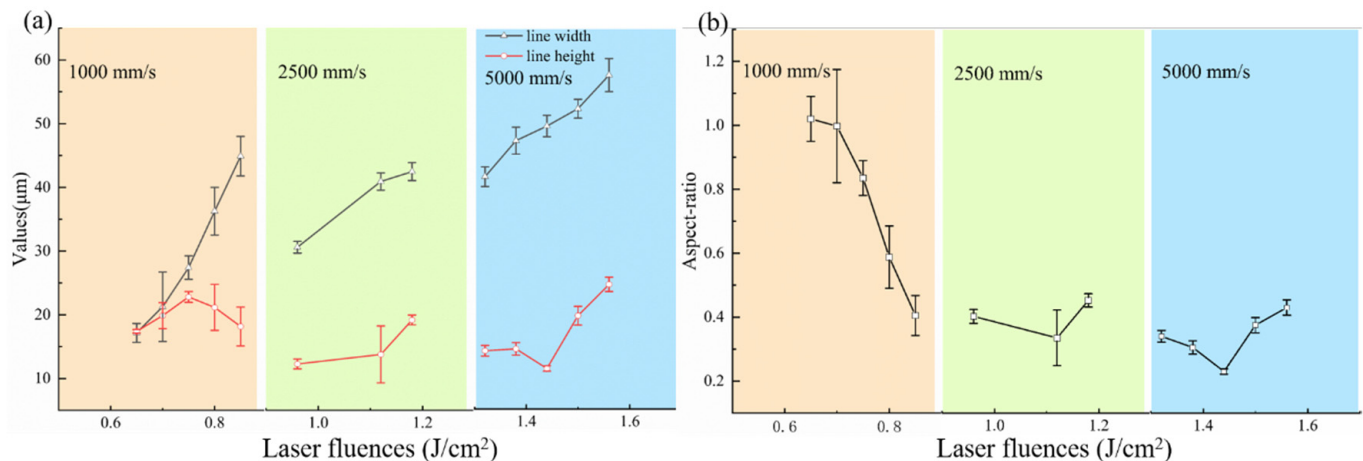


Figure 4. Width, height and aspect-ratio of the formed lines under different laser fluences and processing speeds. (a) line width and line height, (b) aspect-ratio of the formed line.

3.2. Morphological Characteristics of Formed Lines

Morphological characteristics of the formed lines will also have a significant impact on the cell efficiency of silicon wafers. For the formed lines, their cross-sectional area is expected to be enlarged for reducing contact resistance and thus increasing the conductance of the electrode [13,14]. Figure 5 shows the three-dimensional morphology of the formed lines under different laser fluences at the processing speeds of 1000 mm/s , 2500 mm/s and 5000 mm/s , respectively. It can be seen that there were two kinds of line morphology from the perspective of line height. One was high in the middle and low on both sides, namely a single peak; the other was high on both sides and low in the middle, namely a double peak. The line morphology with a single peak was circled by red solid line and that with double peaks was circled by blue solid line in Figure 5. It can be found that at each processing speed, the morphology with a single peak was formed at the critical transfer fluence. The formed line was highest in the middle, accompanied by a gradual rise of the edges. However, when the laser fluence exceeded this critical transfer threshold, it could be noticed that there was a clear shift from single to double peaks in the line morphology. The formed line was high on both sides and low in the middle. Two symmetrical protrusions with steep edges were observed on the silicon wafer.

Cross-sectional profiles of the formed lines varied with laser fluences were measured by LSCM at processing speeds of 1000 mm/s , 2500 mm/s and 5000 mm/s , as shown in Figure 6. As the laser fluence increased, for the formed line with double peaks, the width of central depression area increased. However, the height difference between the middle and edge decreased with the increase of laser fluence. When the laser fluence was much higher than the transfer threshold, explosive transfer occurred, so the characteristic of double peaks was no longer evident. Cross-sectional profile of the formed line became wide and flat. It can be concluded that the change of sectional morphology depended on the laser fluence during the transfer process. The rheological properties of the silver paste and forces acting on it would be affected by laser fluence, which will be discussed in detail in the following section.

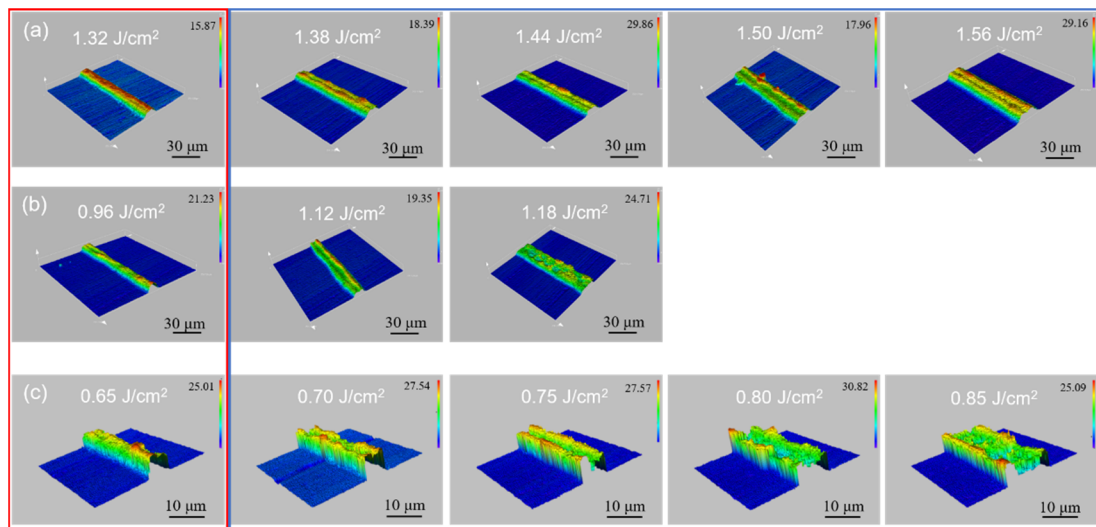


Figure 5. Three-dimensional morphology of the formed lines under different laser fluences and processing speeds obtained by LSCM. (a) 1.32–1.56 J/cm², 5000 mm/s, (b) 0.96–1.18 J/cm², 2500 mm/s, (c) 0.65–0.85 J/cm², 1000 mm/s.

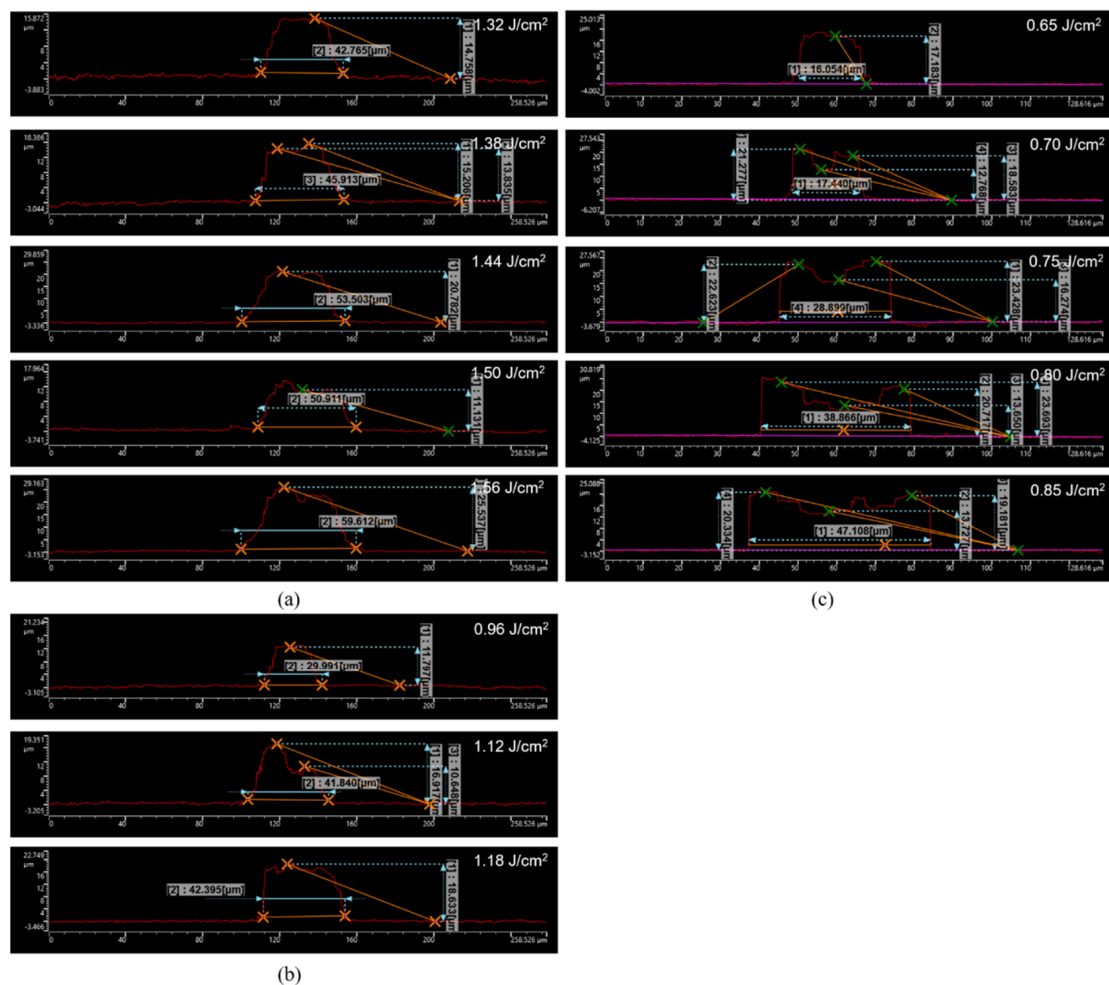


Figure 6. Cross-sectional profiles of the formed lines under different laser fluences and processing speeds obtained by LSCM. (a) 1.32–1.56 J/cm², 5000 mm/s, (b) 0.96–1.18 J/cm², 2500 mm/s, (c) 0.65–0.85 J/cm², 1000 mm/s.

3.3. Dynamics Process of Silver Paste Transfer

There are many donor materials used for laser-induced forward transfer technology. The transfer mechanisms depend on properties of the donor materials and laser beam characteristics, which influence the morphological characteristics of the formed lines in different ways. Thus, the understanding of dynamics process of silver paste transfer is necessary, which is helpful to optimize its complex process parameters.

3.3.1. Formation and Expansion of Bubbles

When the silver paste was irradiated by the laser pulse through the laser-transparent donor, the quick vaporization of the organic component in the silver paste occurred. A bubble was created rapidly due to the high dynamic pressure loading on the interface between donor and silver paste. The chemical kinetics of vapor formation was not considered, since the assumption was established that the vaporization of organic polymer contained in the silver paste was generated immediately under laser irradiation [4]. It was assumed that the size of the initial bubble volume was mainly determined by the laser fluence. After that, the evolution of the bubble was attributed to the balance of internal and external forces. There were two free interfaces for the movement of silver paste, which were bubble-paste interface and paste-air interface, respectively. Firstly, at the bubble-paste interface, the silver paste around the bubble was pushed to expand radially, and a protrusion of silver paste was formed at the paste-air interface. It was then pushed away toward the acceptor due to the evolution of the bubble.

From Sections 3.1 and 3.2, it can be found that there was a critical transfer threshold for the continuous line transfer. Below this threshold, no silver paste was transferred down or there were dots transferred. Only when the laser fluence reached or exceeded the threshold, there were continuous lines transferred onto the silicon wafer. Figure 7 schematically illustrates the dynamic processes of bubble formation and silver paste transfer under different laser fluences.

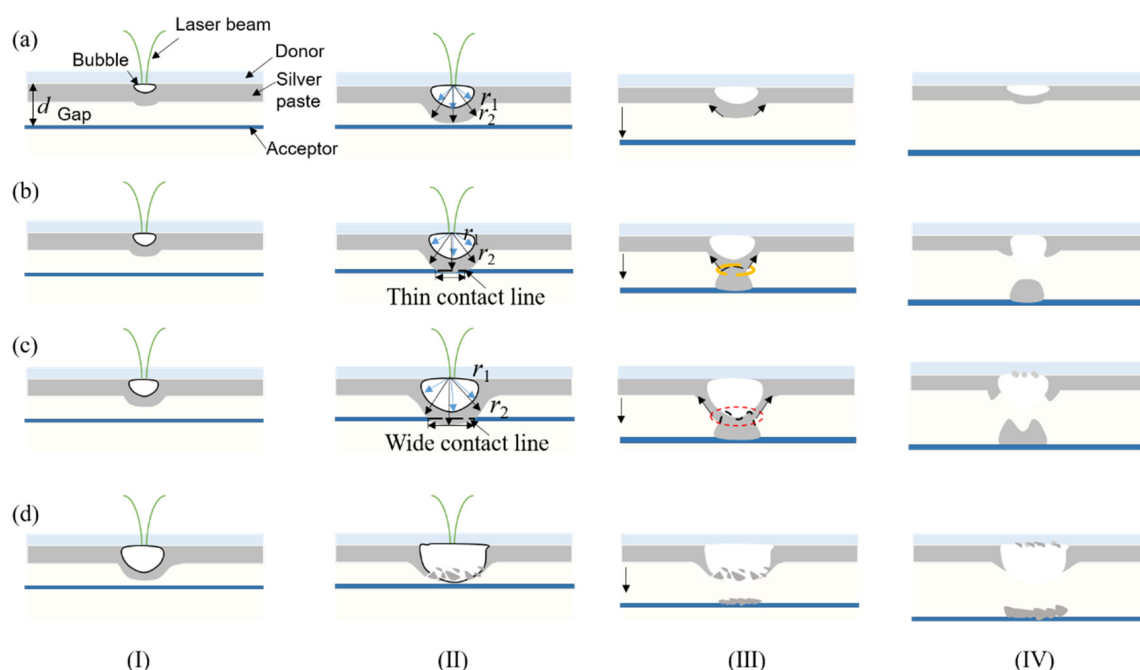


Figure 7. Schematic diagram of dynamic processes for the silver paste transfer under different laser fluences. (a) below critical threshold, (b) critical transfer threshold, (c) above critical threshold, (d) much higher than critical threshold.

The silver paste was mainly driven by the expansion of the bubble induced at the interface between donor and silver paste. The whole transfer process could be divided

into four stages, which were as follows: (I) formation of the small bubble under initial laser irradiation; (II) hemispherical expansion or unstable fragmentation of the bubble in the direction normal to the surface during evolution, and non-contact or contact shown between the acceptor and the bubble; (III) the bubble no longer expanded after laser irradiation was terminated and detachment of the acceptor away from the donor substrate; (IV) solidification of the formed line after the separation of donor and acceptor. In order to demonstrate the variation of the expansion bubble under different laser fluences, geometric morphologies of the remaining silver paste on the donor and the formed lines on the silicon wafer just after the experiment were measured at the processing speed of 1000 mm/s, as shown in Figure 8, and Table 2 shows the comparison of geometric features under different laser fluences.

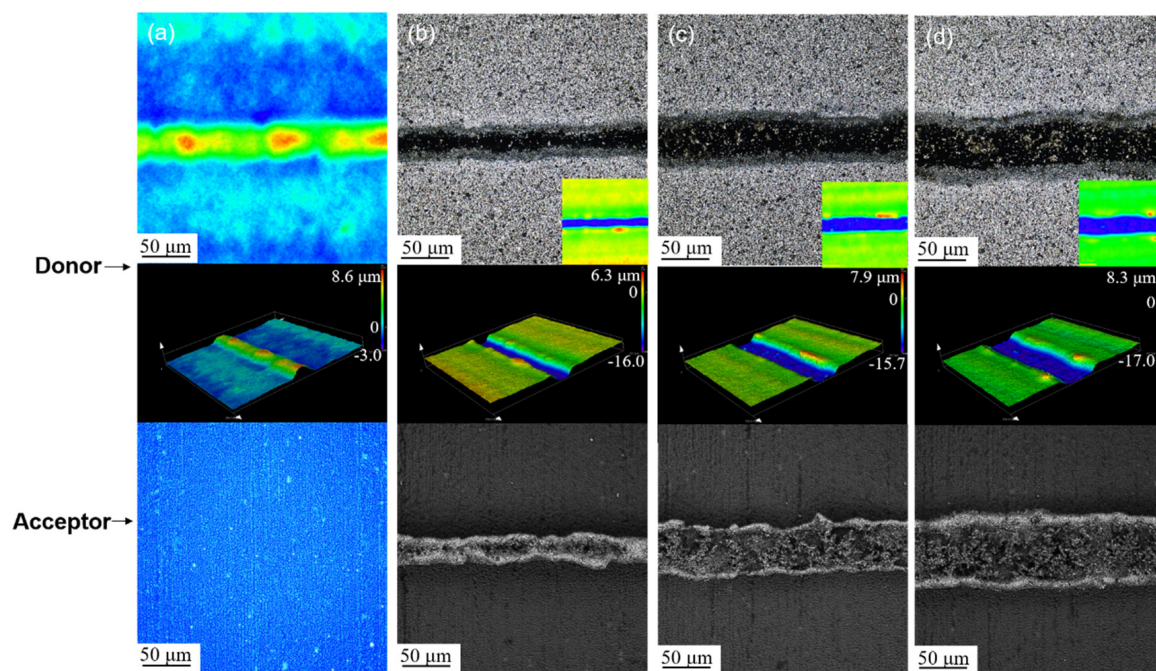


Figure 8. Geometric morphology of the silver paste remaining on the donor and the formed lines (unsintered) on the acceptor, obtained by LSCM. (a) below critical threshold, (b) critical transfer threshold, (c) above critical threshold, (d) much higher than critical threshold.

Table 2. Width and height of the protrusion and formed line on the donor and acceptor under different laser fluences.

		Donor		Acceptor	
No-Transferred		Protrusion Width (μm)	Protrusion Height (μm)	Line Width (Unsintered, μm)	Line Height (Unsintered, μm)
Laser Fluence (J/cm ²)					
Below critical threshold	0.50	34.11	3.08	/	/
	0.55	39.61	4.60	/	/
	0.60	41.62	5.75	/	/
Transferred		Slit Width (μm)	Slit Height (μm)	Line Width (Unsintered, μm)	Line Height (Unsintered, μm)
Laser Fluence (J/cm ²)					
Critical transfer threshold	0.65	36.55	15.77	27.74	27.35
Above critical threshold	0.70	38.08	15.95	34.00	23.70/15.18
	0.75	44.97	16.17	49.35	23.73/20.10
Much higher than critical threshold	0.90	74.34	16.16	77.67	24.03/14.20

From Figure 7a, it can be found that when the laser fluence was below the critical threshold, a small bubble was formed firstly, which was similar to the formation of bubble after the laser beam was focused on a solid polymer film [15]. After the bubble continued to absorb the radiant energy and grew only to a modest size r_1 until the laser beam moved away. The silver paste around the bubble was migrated downward, but the radius of the protrusion r_2 was too small to make it contact with the acceptor. Therefore, there was no transfer of silver paste on the acceptor. Finally, the bubble would totally deflate, leaving a protrusion of silver paste on the donor. Figure 8a and Table 2 show the final width and height of the protrusion for the silver paste remaining on the donor. It can be noticed that the protrusion was continuous along the processing direction of the laser beam. Compared with the initial paste thickness, the size of the protrusion was approximately 3.1–5.8 μm , which was less than the gap between the paste bottom and acceptor. As the laser fluence increased, the width and height of the protrusion increased. This indicated the volume of the induced bubble increased with the increase of irradiation energy.

When the laser fluence just reached the critical transference threshold, a bubble with a modest size was firstly formed due to the increase of irradiation energy. There was higher internal pressure in the bubble, resulting in a larger protrusion of the silver paste around the bubble. As the bubble continued to expand, the height of the protrusion was close to the distance between the paste bottom and acceptor. Eventually, the coherent flow and stretching of paste came into contact with the silicon wafer. An initial contact surface was formed with a certain width and height. It can be observed that almost all of the silver paste around the radiation area was transferred down, leaving a long and narrow slit on the remaining donor, as shown in Figure 8b. There were slight protrusions on both sides of the slit. The width and height of slit on the donor and formed line on the acceptor are shown in Table 2. Here the formed line was not dried and sintered for the comparison of slit and transferred line just after the experiment. The width of the formed line on the acceptor was reduced by about 10 μm compared to that of the slit on the donor. Furthermore, the line height was increased by 11 μm , resulting in the aspect-ratio close to 1. It could be concluded that the silver paste transferred on the acceptor exhibited a retracting characteristic. A stable connecting bridge was formed between the donor and the acceptor. The fracture occurred in the middle of the connecting bridge when separating the donor from the acceptor. The width here was significantly smaller than that of the slit left on the donor. The retraction characteristic of the transferred silver paste was largely related to laser fluence, surface tension and viscosity force.

When the laser fluence was above the critical transfer threshold, a larger bubble was formed firstly. However, the increase in the difference between internal and external pressure was not sufficient to cause explosion of the bubble. The subsequent dynamic evolution of the bubble and silver paste were similar to that at the critical transference threshold, as seen in Figure 7c. The radially outward motion of silver paste was induced by a larger bubble, which led to a larger contact area with the acceptor. A long and wider slit was formed on the remaining donor, as shown in Figure 8c. Compared with Figure 8b, there were many scattered silver particles and clusters distributed in the middle of the slit. This might be due to the large recoil of the downward expanding bubble. Some paste was backflushed and left on the donor substrate. The width of slit and formed line increased with the increase of laser fluences. However, the slit height was almost constant, between 15–16 μm . This was because when the silver paste was completely transferred down, the slit height was determined by the thickness of the coating film. The two heights of one formed line are presented in Table 2 because it has double peaks in the cross section.

For the laser energy much higher than the critical fluence, a more violent bubble was produced. The higher inner pressure would be applied on the bubble-paste interface, which was capable to overcome the capillary force and break the bubble wall leading to burst [4]. Then the protruding silver paste was quickly broken into a few clumps of paste, with many small clumps propelled away from the donor to the acceptor. An explosive phenomenon occurred during the whole transfer process, resulting in the formation of a wider slit and

formed line, as seen in Figures 7d and 8d. The height of the slit and formed line remained almost unchanged. However, when the laser fluence was much higher than the critical threshold, the formed line was wider than the slit. The silver paste transferred on the acceptor exhibited a stretching characteristic. Because of higher pressure, many silver paste fragments were expelled away from around the bubble. They were unstable and could be broken up, with a wide distribution. It is shown that the silver paste reached the acceptor while exploding, leaving a flat deposit with a certain height and covering a large area on the silicon wafer with larger width.

3.3.2. Formation of Single and Double Peaks

The gap between the donor and acceptor plays an important role in the transfer process of silver paste and formation of silver line, especially when the gap is small enough compared with the paste thickness. The protruding silver paste reaches the acceptor, at the same time it is connected to the donor, due to its high viscosity and normal yielding stress. Unlike low-viscosity silver pastes or inks, the high-viscosity silver paste is bound by large surface tension and viscous forces during the evolution process. The expansion of the silver paste will be prevented once it has struck the acceptor. A stable and connected bridge similar to the liquid bridge was formed due to the existence of the confinement of acceptor. Then, final morphology of the formed line is obtained after the donor is removed away from the acceptor.

In this paper, the viscosity of silver paste was very high and the gap between the paste bottom and acceptor was small, close to one-third of the paste thickness. From Section 3.2, it can be found that at the critical and above transfer threshold, the silver paste was transferred with cross-sectional morphologies of single and double peaks, respectively. The variation of sectional morphology was closely related to the transfer dynamics of silver paste on the acceptor. In order to explain this phenomenon, it is desirable to analyze and understand the forces on the silver paste during the transfer process. A schematic diagram of the forces is shown in Figure 9. In principle, the silver paste is a multiphase fluid. For simplicity, it was considered as consisting of two parts: more than 90% solid particles and a small amount of organic solvent. It was assumed that the mass was conserved during the downward transfer.

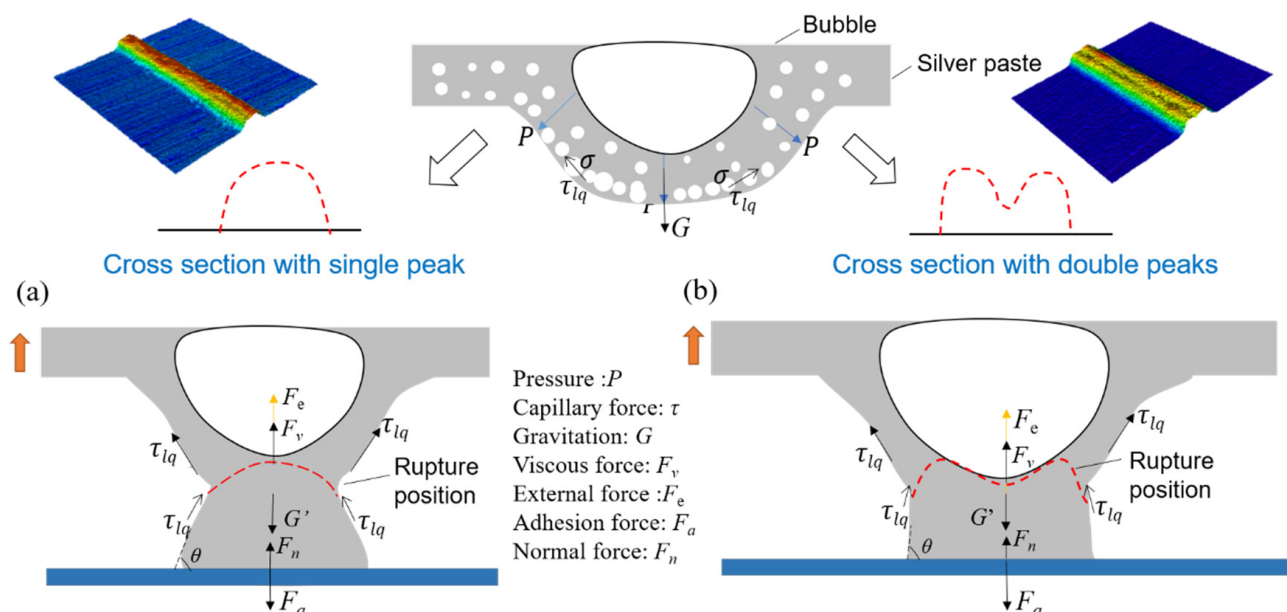


Figure 9. Schematic diagram of the forces on the silver paste at the bottom of the bridge during the transfer process. (a) forces on the silver paste when the laser fluence was at critical transfer threshold, (b) forces on the silver paste when the laser fluence was above transfer threshold.

Due to the shear thinning properties of the silver paste, the viscosity around the bubble decreased as the bubble expanded downward rapidly. It was assumed that the transfer process had no voxel rotation and no shear force was considered. The silver paste was bulged downward under the action of pressure P , gravity G and capillary force τ . It came into contact with the acceptor as the bubble evolved. The viscosity of silver paste would increase after the loss of kinetic energy. A bridge between the silver paste and acceptor was established, as shown in Figure 9a,b. The adhesion force F_a was enhanced with the wetting process of silver paste filling onto silicon wafer. A high mechanical interlocking was formed between the silver paste and acceptor, which favored the formation of the stable bridge [16]. After contact, the bubble began to deflate as the difference between internal and external pressure decreased. After complete deflation of the bubble, the donor removal was done, and steady state reached. The donor was detached away from the acceptor by an external force F_e perpendicular to the bridge. This connection was disrupted, leaving the silver paste on the lower side of the bridge to be transferred onto the acceptor. The protrusion of silver paste on the acceptor could remain for milliseconds because of its high viscosity. The capillary force τ would tend to make the top of formed line more uniform and flat.

For the silver paste on the bottom of the bridge, when the combined force (F_e , τ , normal force F_n , and viscous force F_v induced by the top silver paste) in the axial upward direction was greater than that (G , F_a) in the axial downward direction, the bridge fractured. The volume of the expansion bubble was closely related to the laser fluence. At the critical transfer threshold, the volume of the expansion bubble was moderate and part of silver paste was dragged from the donor and transferred onto the acceptor, leading to a narrow bridge. The rupture position occurred in the middle along the height direction under the action of forces, but it did not touch the bottom of the bubble and the silver paste was transferred down in the form of single peak. When the laser fluence was above the transfer threshold, the volume of the bubble was much larger than that at the critical transfer threshold, until the silver paste touched the acceptor. More silver paste was dragged from the donor and transferred onto the acceptor, leading to a wider bridge. The external force F_e was required to separate donor and acceptor. The rupture of the bridge occurred in the middle, where almost no silver paste was present due to the contact of the rupture location with the bottom of the large expansion bubble. Thus, a collapse in the middle of the transferred silver paste was created, exhibiting the line morphology with double peaks.

For the silver paste metallization, the overlap rate is considered with other processing parameters together, such as laser fluence, scanning speed, repetition rate, film thickness and gap distance. Only when the right matching interval is found, can a continuous line be transferred. The gap distance from the bottom of the silver paste to the acceptor is much smaller than the film thickness. This is quite different from the previous references [4,5,11]. In the case of small gap, the continuous protuberance of the silver paste around the bubble can touch the acceptor. A stable connecting bridge can be generated under the continuous pulse overlap so the continuous lines can be transferred. To some extent, the printing problems at high overlap can be overcome. It is vital to select the proper processing windows. It was proved that the continuous grid lines could be formed by laser-induced forward transfer, when the laser fluence reached the critical or above the transfer threshold. Silver lines with narrow width and large aspect-ratio could be obtained only at the critical laser fluence. The formed line was presented with the cross-sectional morphology of single peak at this fluence, which helps to enlarge the sectional area for increasing electrode conductance. Moreover, transfer mechanisms using high-viscosity silver paste and small gap were discussed under different laser fluences. This work provides a guide on the transfer of grid lines of solar cells in the photovoltaics industry. In the future, the dynamic evolution behaviors of silver paste and driving mechanism of the bubble will be further investigated based on in-situ observation and numerical simulation.

4. Conclusions

In this work, a study on laser direct forming of silver lines was performed for metallization of solar cells. The silver paste with high viscosity and solid content, and relatively small gap between the donor and acceptor were used to transfer grid lines on silicon wafers. The morphological characteristic of the formed line under different laser fluences and processing speeds were discussed. Different transfer mechanisms were revealed by comparing the silver paste remaining on the donor and transferred to the acceptor. Some conclusions can be highlighted as follows:

- There was a critical laser fluence for the continuous line transferred. Different transfer states were observed under different laser fluences: non-formed lines or formed but no continuous lines (below threshold), continuous formed lines (critical and above threshold), and explosive formed lines (much higher than the critical threshold).
- At the processing speeds of 5000 mm/s, 2500 mm/s and 1000 mm/s, the critical transfer thresholds were 1.32 J/cm², 0.96 J/cm², and 0.65 J/cm², respectively. A larger transfer threshold was required at higher processing speeds. As the laser fluence increased, the line width increased significantly.
- For the continuous line transfer, cross-sectional morphologies of the formed line with single and double peaks were observed at the critical and above transfer threshold, respectively. The highest point of single peak appeared at top of the protrusion, accompanied by a gradual rise of the edges. While two symmetrical protrusions with steep edges were shown for the formed line with double peaks. The height difference between the middle and edge decreased with the increase of laser fluence.
- By comparing the silver paste remaining on the donor and transferred to the acceptor, it was found the silver paste transferred on the acceptor exhibited a retracting characteristic under the critical and above the transfer threshold. While a stretching characteristic was exhibited when the laser fluence was much higher than the transfer threshold. Under the action of the axial combined forces (G , τ , F_v , F_e , F_a , and F_n), the distance between the rupture position of the bridge and the bottom of the bubble determined the morphological characteristics of single or double peaks.

Author Contributions: Conceptualization, Y.Z., C.T., Y.Y., X.H., S.L. and G.Y.; methodology, Y.Z., C.T., Y.Y., X.H., Y.B., S.L. and G.Y.; software, Y.B.; validation, X.H. and G.Y.; formal analysis, Y.B.; investigation, Y.Z., C.T., Y.Y. and S.L.; resources, C.T.; data curation, Y.Z., C.T. and Y.Y.; writing—original draft, Y.Z.; writing—review & editing, Y.Z. and X.H.; visualization, Y.Z. and Y.B.; supervision, X.H., S.L. and G.Y.; project administration, S.L. and G.Y.; funding acquisition, S.L. and G.Y. All authors have read and agreed to the published version of the manuscript.

Funding: This work was supported by the Research Project of Guangdong Aerospace Research Academy Research Project (GARA2022001000).

Institutional Review Board Statement: Not applicable.

Data Availability Statement: Not applicable.

Conflicts of Interest: The authors declare no conflict of interest.

References

1. Shan, Y.; Zhang, X.; Li, H.; Zhan, Z. Single-step printing of high-resolution, high-aspect ratio silver lines through laser-induced forward transfer. *Opt. Laser Technol.* **2021**, *133*, 106514. [\[CrossRef\]](#)
2. Gupta, N.; Rao, K.D.M.; Gupta, R.; Krebs, F.C.; Kulkarni, G.U. Highly Conformal Ni Micromesh as a Current Collecting Front Electrode for Reduced Cost Si Solar Cell. *ACS Appl. Mater. Interfaces* **2017**, *9*, 8634–8640. [\[CrossRef\]](#) [\[PubMed\]](#)
3. Adrian, A.; Rudolph, D.; Willenbacher, N.; Lossen, J. Finger Metallization Using Pattern Transfer Printing Technology for c-Si Solar Cell. *IEEE J. Photovolt.* **2020**, *10*, 1290–1298. [\[CrossRef\]](#)
4. Sopena, P.; Fernández-Pradas, J.M.; Serra, P. Laser-induced forward transfer of conductive screen-printing inks. *Appl. Surf. Sci.* **2020**, *507*, 145047. [\[CrossRef\]](#)
5. Munoz-Martin, D.; Chen, Y.; Morales, M.; Molpeceres, C. Overlapping Limitations for ps-Pulsed LIFT Printing of High Viscosity Metallic Pastes. *Metals* **2020**, *10*, 168. [\[CrossRef\]](#)

6. Delaporte, P.; Alloncle, A.P. [INVITED] Laser-induced forward transfer: A high resolution additive manufacturing technology. *Opt. Laser Technol.* **2016**, *78*, 33–41. [\[CrossRef\]](#)
7. Arnold, C.B.; Serra, P.; Pique, A. Laser direct-write techniques for printing of complex materials. *MRS Bull.* **2007**, *32*, 23–31. [\[CrossRef\]](#)
8. Serra, P.; Pique, A. Laser-Induced Forward Transfer: Fundamentals and Applications. *Adv. Mater. Technol.* **2019**, *4*, 1800099. [\[CrossRef\]](#)
9. Biver, E.; Rapp, L.; Alloncle, A.-P.; Delaporte, P. Multi-jets formation using laser forward transfer. *Appl. Surf. Sci.* **2014**, *302*, 153–158. [\[CrossRef\]](#)
10. Patrascioiu, A.; Florian, C.; Fernandez-Pradas, J.M.; Morenza, J.L.; Hennig, G.; Delaporte, P.; Serra, P. Interaction between jets during laser-induced forward transfer. *Appl. Phys. Lett.* **2014**, *105*, 014101. [\[CrossRef\]](#)
11. Sanchez-Aniorte, M.I.; Mouhamadou, B.; Alloncle, A.P.; Sarnet, T.; Delaporte, P. Laser-induced forward transfer for improving fine-line metallization in photovoltaic applications. *Appl. Phys. A-Mater. Sci. Process.* **2016**, *122*, 595. [\[CrossRef\]](#)
12. Shan, Y.; Zhang, X.; Chen, G.; Li, K. Laser induced forward transfer of high viscosity silver paste on double groove structure. *Opt. Laser Technol.* **2022**, *148*, 107795. [\[CrossRef\]](#)
13. Zhou, Y.Y.; Tong, H.; Liu, Y.J.; Yuan, S.L.; Yuan, X.; Liu, C.; Zhang, Y.C.; Chen, G.R.; Yang, Y.X. Rheological effect on screen-printed morphology of thick film silver paste metallization. *J. Mater. Sci.-Mater. Electron.* **2017**, *28*, 5548–5553. [\[CrossRef\]](#)
14. Green, M.A. Third generation photovoltaics: Ultra-high conversion efficiency at low cost. *Prog. Photovolt. Res. Appl.* **2001**, *9*, 123–135. [\[CrossRef\]](#)
15. Kattamis, N.T.; Brown, M.S.; Arnold, C.B. Finite element analysis of blister formation in laser-induced forward transfer. *J. Mater. Res.* **2011**, *26*, 2438–2449. [\[CrossRef\]](#)
16. Chen, Y.; Morales, M.; Munoz-Martin, D.; Molpeceres, C. Influence of the acceptor roughness on the aspect ratio of silver paste lines printed by laser-induced forward transfer. *Results Phys.* **2016**, *6*, 998–999. [\[CrossRef\]](#)